High gradient Terahertz-driven ultrafast photogun

Jianwei Ying[1†], Xie He[1†], Dace Su[1], Lingbin Zheng[1], Tobias Kroh[2], Timm Rowher[2], Moein Fakhari[2], Günther Kassier[2], Jingui Ma[1], Peng Yuan[1], Nicholas H. Matlis[2], Franz X. Kärtner[2*] and Dongfang Zhang[1*]

Affiliations:

[1]Key Laboratory for Laser Plasmas (Ministry of Education), Collaborative Innovation Center of IFSA (CICIFSA), School of Physics and Astronomy, Shanghai Jiao Tong University, Shanghai 200240, China

[2]Center for Free-Electron Laser Science, Deutsches Elektronen Synchrotron, Notkestrasse 85, 22607 Hamburg, Germany

*To whom correspondence should be addressed. E-mail: franz.kaertner@desy.de; dongfangzhang@sjtu.edu.cn

†Equal contribution.

Abstract

Terahertz (THz)-based electron acceleration has the potential as a technology for next-generation cost-efficient compact electron sources. Although proof-of-principle demonstrations have proven the feasibility of many THz-driven accelerator components, THz-driven photoguns with sufficient brightness, energy, and control for use in demanding ultrafast applications have yet to be achieved. Here, we present a novel millimeter scale waveguide-based THz-driven photogun that exploits field enhancement to boost the electron energy, a movable cathode to achieve precise control over the accelerating phase as well as a multifunction cavity for exquisite beam control. The short

driving wavelength enables a peak acceleration gradient as high as ~3 GV/m. Using microjoule-level single-cycle THz pulses, we demonstrate electron beams with up to ~14 keV electron energy, 1% energy spread and ~0.015 mm mrad transverse emittance. With a highly integrated rebunching cavity the bunch is further compressed by about 10 times to 167 fs with ~10 fC charge. High-quality diffraction patterns of single crystal silicon and projection microscopy images of the copper mesh are achieved. We are able to reveal the transient radial electric field developed from the charged particles on a copper mesh after photoexcitation with high spatiotemporal resolution, providing a potential scheme for plasma-based beam manipulation. Overall, these results represent a new record in energy, field gradient, beam quality and control for a THz-driven electron gun, enabling for the first-time real applications in electron projection microscopy and diffraction. It is therefore a critical step and milestone in the development of all-optical THz-driven electron devices validating the maturity of the technology and its use in precision applications.

Introduction

Today, ultrashort electron bunches are widely employed for a large range of applications ranging from ultrafast electron diffraction[1-3], and microscopy[4,5] to ultrafast x-ray sources[6]. Radio-frequency (RF) (1–10 GHz) based accelerators have been the conventional choice for accelerating electrons. However, RF-based accelerators require costly infrastructure of large size and power, limiting their availability to a broader scientific community. Therefore, there is a strong motivation for exploring novel compact technologies that promise not only lower cost, but may eventually achieve higher spatio-temporal resolution. Prime examples are laser-plasma accelerators (LPAs)[7-9], dielectric laser accelerators (DLAs)[10,11] and terahertz- (THz-) driven accelerators[12-19]. Both LPAs and DLAs can generate extremely high acceleration gradients on the order of GV/m. However, LPAs suffer from instabilities and difficulties in controlling beam parameters due to the

dynamical nature of the plasma, and DLAs require extreme tolerances in beam control and are limited to near single-electron bunches due to their submicron-scale cross sections. As a result, these technologies have yet to be employed for practical applications.

Recently, there has been significant interest in the use of THz-based particle acceleration and beam-manipulation. The millimeter scale devices provide a compromise between the meter-scale RF- and the micron-scale other laser- based technologies. Compared with RF-based accelerators, THz-based accelerators are driven by higher frequencies and shorter-duration pulses which promise to enable greater acceleration gradients in the range of GV/m[19-26], hence, allowing devices to shrink significantly in size, cost and infrastructure. In addition, the use of optical methods for THz generation provides intrinsic synchronization between the electrons, the driving fields, and probe lasers, providing opportunities for achieving an exquisite level of timing control[27]. Proof-of-principle demonstrations have shown multiple tens-of-keV electron acceleration[12-16] in THz-driven modules seeded by conventional DC- and RF- guns. Other functions such as electron compression, focusing, and streaking have also been demonstrated[12,13,28,29]. However, the exploration of THz acceleration technology is still in its infancy, leaving many critical gaps that limit its widespread use in practical applications such as ultrafast electron microscopy and diffraction.

In particular, a THz-driven photogun of appreciable performance proving its practical application has yet to be demonstrated. Photoguns, which represent the electron sources are a key element of most accelerators. Development of high-quality photoguns is generally challenging due to the dramatic changes in the speed of the electrons and the sensitivity to Coulomb repulsive forces during the initial phases of acceleration. Scaling up to THz frequencies means reducing the physical scale of the device and the interaction length by orders of magnitude which brings

additional challenges. Among these are: 1) controlling the driving field and emission of electrons, hence the interaction, to a volume small enough to prevent the initially-slow electrons from "dephasing" (i.e., outrunning the accelerating phase of the wave); 2) providing sufficient concentration of the THz energy to enable high field acceleration; and 3) Manipulating (focusing, compression, etc.) the electron beam in the millimeter scale cavity for high-quality electron beam generation and practical applications.

Early work on THz-driven electron sources has explored the use of nanotips to generate strongly localized fields[30-32]. However, the total energy gain was limited by the extremely short (10s of nanometers) interaction lengths and dephasing and the number of electrons is limited to a few electrons per pulse[30]. Acceleration cavities have been explored to address the dephasing issues and extend the interaction length[33]. In 2016, Huang et al. demonstrated a single-layer device by using a parallel-plate waveguide structure[34]. The interaction region, however, was still too long for the short dephasing length set by the driving wavelength, resulting in cycling between acceleration and deceleration that limited the energy to below 1 keV. The beam quality is also influenced by the nonuniform field distribution generated by the single side pumped THz wave. In the meantime, although different functions (acceleration, compression, focusing etc.) have been demonstrated in THz-driven devices, effective integration of multiple functions has yet to be demonstrated. There is still a lack in machining precision and control capability within the millimeter region that leads to poor beam quality (large energy spread and emittance, long electron bunch etc.), hence, limiting the potential of THz guns for future compact light sources and practical applications in ultrafast electron microscopy and diffraction[35,36].

In this letter, we demonstrate a novel concept which combines the advantages of nanotips and multifunction waveguide approaches and, in addition, adds a degree of tuning of the cathode which

critically addresses the dephasing issue and beam control. A movable, micrometer size tip-shaped cathode is integrated into a multi-layer, waveguide-based device allowing for a small, continuously tunable interaction length for acceleration that is more easily adaptable to varying THz energies. The horn coupler enables sub-wavelength concentration of the THz wave. With the enhancement of the tip-cathode, extreme field gradients as high as 3 GV⁄m have been achieved. Using only a few-microjoules of single-cycle THz radiation, we demonstrate electron beams with ~14 keV electron energy, 1% energy spread and 0.015 mm mrad transverse emittance focusable down to a beam diameter of ~90 μm (rms). For the first time, multifunction (acceleration and compression) has been integrated into the same sub-millimeter scale device, resulting in a compressed electron bunch of ~ 167 fs (rms). We were able to achieve high quality projection microscopy images on copper mesh and diffraction on single crystal silicon. The relative low electron energy enables high sensitivity to the field dynamics. This enables us to map the transient field developed by the positively and negatively charged particles after photoexcitation on a copper mesh with high spatial and temporal resolution, paving the way for precision control of beams with well-designed plasma fields. The implementations of the THz-driven device in microscopy and diffraction validates the maturity of THz-driven ultrafast electron sources for use in precision applications. These results represent the highest overall energy, acceleration field gradient and quality so-far reported from an all-optical THz-powered device and paves the way for future implementations for other research areas such as tabletop radiation sources.

Concept and implementation

The experimental setup (Fig. 1) consists of three single-cycle THz generation stages, a THz-powered photogun, a UV pulse, and one pump laser for sample excitation, all of which were driven by the same IR laser source. UV pulses for photoemission were generated by two successive

second harmonic generation stages in BBO crystals. Single-cycle THz pulses were generated by optical rectification in lithium niobate crystals using the tilted-pulse-front method [20]. The THz pulses from two independent setups were then coupled into the device transversely by two horn structures which concentrate the counter-propagating THz waves into the sub-wavelength interaction zone. The third THz wave is used for bunch length measurement. The tip-cathode is made out of tungsten and mounted on a precision motorized stage for photoelectron generation.

Two THz pulses are coupled into the device from the sides (Fig. 1) through symmetric horn structures with the electric field set parallel to the electron propagation direction. Upon entering the interaction region, the electrons experience the electric field for acceleration/deceleration and magnetic fields for deflection according to the Lorentz force law. For clean electric field interaction, the two counter-propagating THz pulses are set to ensure that the electric field constructively interferes at the interaction point, while the magnetic fields are 180° out of phase and cancel each other. Their relative timing can be precisely controlled by tuning the delay of the two THz pulses and the electron emission via the motorized stages for each relative IR and UV beam. The relative delay between the two counter-propagating THz pulses sets the accelerating field, while the UV delay controls the injection phase into the THz accelerating field. In order to achieve simultaneously high energy and short electron bunches, inside the device, cascaded acceleration and compression are introduced. The THz beams are split transversely by thin metal sheets into two beams (Fig. 1 Inset), each guide in a THz waveguide carrying a fraction of the total energy to the interaction region. In the first waveguide, the UV delay controls the injection phase into the THz accelerating field. The tip-cathode introduces field enhancement and its distance to the anode determines the THz-electron interaction length. A micrometer size tip-cathode instead of nanotip is used to obtain micrometer acceleration length. The movable tip-cathode design

ensures that the electron bunch only experiences the negative cycle of the THz electric fields, resulting in a net, continuous acceleration. In the second layer, dielectric slabs with tailored lengths are inserted to match the arrival time of the THz wavefront with that of the electrons. Therefore, the electrons are timed to travel through the zero-crossing of the THz field, that causes acceleration of the electron bunch tail and deceleration of the bunch head, leading to ballistic longitudinal focusing.

For electron energy measurements, an electromagnetic dipole was used to induce energy-dependent deflections. The mean energy of the electron bunch is cross calibrated with the focusing solenoid by comparing the focusing strength applied to electron bunches at different energy. The energy and spatial profile of the accelerated electrons were analyzed using a microchannel plate (MCP) and phosphor screen that was monitored by a CCD camera (see Fig. 1). The amount of charge in this experiment is ~10 fC/shot measured by a faraday cup. The charge was also increased by ~10 times and there was no degradation of the cathode over several hours of operation.

Results

Controlled, tip-enhanced photogun

The capability of precise phase control through the controlled tip-cathode is first demonstrated in a single-layer gun [see Supplementary Information for detailed design parameters] through the electron yield and energy measurement. By scanning the relative delay of the UV and the two THz pulses, we can map out the parameter space associated with acceleration as shown in Fig. 2. The points with high signal correspond to the coincidence of photoexcited electrons and THz electric superposition. The strongest signal occurs for zero delay in the vertical axis which corresponds to symmetric optical paths for the two THz pulses and hence electric superposition (and magnetic

cancellation) of the primary peaks from the two THz waveforms. Other high-signal points at different THz delays correspond to electric superposition between peaks of differing index from the two arms (e.g., the first peak of one arm with the second peak of the other). Similarly, high-signal points at different UV delays correspond to the set of points corresponding to electric superposition between peaks with a fixed relative index. Figure 2b shows the Fourier-transformed interference signal (white line in Fig.2a) indicating that the THz pulses coupled from free space into the gun have a center frequency of ~ 150 GHz. Although the THz pulses injected into the device were nearly single cycle, several cycles of acceleration were observed due to the dispersion induced by the relative long waveguide and unmatched coupling angle between the THz and the horn coupler. This can be further improved with a proper coupler design[37], which will not only reduce the dispersion but also increase the field gradient in the interaction region.

Benefiting from the transverse geometry, efficient interaction of the electrons with the acceleration fields can be further optimized by the tip-cathode control. A translation stage is used to adjust the tip-cathode to anode distance with sub-micrometer precision that helps to maximize the emission of electrons at the optimum acceleration phase of the THz wave. Figure 2c shows the electron emission map with different tip-cathode positions versus the relative delay between the UV pulse and the two THz pulses. The highest electron yield was found at a tip-cathode position of 15 μm and zero-time delay between the UV and two THz pulses as shown in Fig. 2c.

The proper acceleration field can be found from the above electron emission map measurement (Fig. 2). At zero-time delay between the two counter-propagating THz pulses, the electric field is maximized with the magnetic field canceled at the center of the interaction region, which ensures clean electric field acceleration. Hence, for energy measurements, the THz delay is fixed at zero-time delay and only the UV delay is adjusted to optimize the injection phase. The energy spectra

of the emitted electrons as a function of the UV delay is measured with an electromagnetic dipole. The resulting spectra are shown in Fig. 3a.

Different tip-cathode positions are also recorded in the electron energy measurement as shown in Fig 3c and 3d. The tip-cathode at 15 μm provides the highest electron energy (Fig. 3c, 3d), which is very close to the point for maximum electron yield (Fig. 2c). While moving away from the optimal position (15 μm), there is a decrease of the energy gain and an increase of the energy spread as the acceleration field is getting lower and dephasing is setting in faster. This finding clearly shows that an offset of the cathode position of only a few micrometers, which is already within the limitations of fabrication with modern mechanical machining tools, may lead to a significant reduction in electron yield and energy, which further implies the importance of precision cathode control.

THz power dependence is also explored as shown in Fig. 3e,f. Using approximately 2×7 μJ single cycle THz pulses, a maximum electron energy of about 1.6 keV is achieved. Lower energetic THz pulses lead to smaller electron energy and larger energy spread (Fig. 3e,f). At the same time, for lower electron energy the influence of space charge limitations are more pronounced[38] which increases the energy spread. In Fig. 3e,f, as the energy difference is small, the difference in the optimal tip-cathode position between the three measured cases is very small (around 1 μm). However, for higher THz energy, the tip-cathode position needs to be shifted. For optimum performance, in the case of a small driving THz energy, the field gradient is low and the electron beam propagates at a slower speed. Dephasing happens within a shorter interaction length. The tip-cathode should be moved closer to the anode to prevent deceleration. Vice versa, for higher THz energy, the tip-cathode to anode distance should be increased to get a longer interaction length, hence larger electron energy. To compare the acceleration process with different tip-

cathode positions, we modeled the propagation of electrons (Fig. 3b). While moving away from the optimal position, the energy gain is reduced due to the faster dephasing and lower field gradient as shown in Fig. 3b. The highest energy gain with the relative tip-cathode position also matches the experimental results very well, as shown in Fig. 3b. Considering the standard machining and assembly precision of a few tens of micrometers, such an offset will lead to an energy decrease of more than 50 %. The movable tip-cathode design can effectively ease these limitations and ensures that the electron bunch interacts in an optimum way with the accelerating THz pulse to maximize acceleration and avoid deceleration. For a practical design, the field gradient, the tip-cathode position, and the interaction length should be balanced and a complete mapping for the tip-cathode position, UV, and THz delay is required for optimum energy and electron emission.

Benefiting from the movable tip-cathode design, the same device also works for other wavelengths. With a shorter wavelength [see supplementary material Fig. S1], under the same field gradient, the tip-cathode distance must be reduced to the anode to maintain a continuous acceleration. The movable tip-cathode provides high flexibility that can be adopted to different THz pulse energies and wavelengths.

High field acceleration

From the initial experiment it shows that the overall interaction length is within a few tens of micrometers with the available THz energy. The first acceleration layer is further reduced to 100 μm, hence, concentrating the field into a smaller region to achieve a higher field gradient. The horn coupler is also redesigned to match the terahertz injection angle, therefore, improving the coupling into the acceleration mode. Figure 4a is the simulated cross section of the field distribution with a tip-cathode considering the coupled THz energy and measured electron energy. With 2*8 μJ THz energy, the maximum peak field reaches around 3 GV/m. It is just below the measurable field

emission threshold of the tungsten tip-cathode[39]. We start to see clear field emission at ~4 GV/m. The field on the tip-cathode is roughly 10 times the highest surface electric field elsewhere in the structure. With this acceleration field, a maximal electron energy of 14 keV is achieved (Fig. 4b). The measured energy spread reaches about 1% (rms), which is also the best so far reported from a THz driven photogun.

The early state of the R&D into THz-driven photoguns is evidenced first by the small number of articles in this field and second by the fact that so far none has reported on the key parameters of transverse emittance and temporal duration of the electron bunches. Here, aided by the achievement of a high-quality electron beam profile (Fig. 4c), we report on these quantities for the first time for a THz-driven photogun. The transverse emittance of the electron bunch is measured by scanning the current of a focusing solenoid and measuring with an MCP detector, the size of the electron beam profile which can be focused down to below 90 μm (rms) beam diameter at its smallest point. Least-square fit is used in the solenoid scan[40], revealing a transverse emittance in the horizontal (red) and vertical (blue) directions of $\varepsilon_{x,n} = 0.014$ mm mrad and $\varepsilon_{y,n} = 0.015$ mm mrad, respectively, as shown in Fig. 4c, which is also a record low emittance reached with a THz-driven photogun.

Integrated multifunction THz-driven device

Ultrafast electron beams enable us to capture the atomic structure of matter and provide structural information on nonequilibrium states of matter on the femtosecond time scale. The major challenge for generating short electron bunches is to overcome the inherent space-charge broadening especially for low energy electrons. Post-compression has been widely used to achieve fs electron bunches in conventional larger scale electron sources[41-44]. For low energy electron beams, electron compression is expected to be implemented directly after acceleration in order to

avoid excessive expansion of the bunches which then sample unwanted emittance-spoiling curvature of the driving waveform in downstream components. In the meantime, for the THz-driven photogun, a higher degree of integration is desired to maintain compactness. Here we designed for the first time a highly integrated multi-function millimeter scale device with cascaded acceleration and compression.

The THz beams are split into two waveguides (Fig. 1 Inset), with the first waveguide for acceleration and the second waveguide for rebunching [see Supplementary Information for detailed design parameters]. Higher degrees of integration lead to more compact devices, however, lower the freedom of phase control between THz-electron interaction as the injection phase and field gradient between acceleration and compression stage are coupled. The movable tip-cathode provides extra freedom by allowing fine tuning of the energy, and hence time-of-flight of the electron beam, which then provides a means of tuning the injection phase into the compression layer, providing a longitudinally-varying energy kick for velocity bunching. The field gradient in the second rebunching waveguide is much lower without the tip. As the electron beam already reaches ~20% of the speed of light, c, in the first waveguide, it enables a much longer interaction length in the second waveguide. In the meantime, once the electrons reach high energy, they become more tolerant against small deviations in fabrication[33], hence, lowering the requirement of fabrication precision in the second waveguide. Compression of the bunch is shown in Fig. 5a and b, which is measured with the THz-based streaker with a metallic slit[45,46]. The streaker uses the electric field of the THz to induce the transverse deflection of the electron beam. When the electrons sweep the zero crossing of the field, they experience a strong deflection as a function of delay, enabling the measurement of the temporal bunch profile by mapping it onto the spatial dimension of a detector. A clear correlation between the bunch length and electron energy is also

observed (Fig. 5c-d). The overall system performance should be optimized by the precise manipulation of the tip-cathode distance, THz field gradient and injection phase. At maximum compression, the electron bunch length reaches around 167 fs (RMS) with 10 keV electron energy and 10 fC charge. The bunch length is ~ 10 times smaller than in the case without compressor which also in good agreement with the simulations (Fig. 5b). Without buncher, the low energy electron bunch quickly extend to several ps within a few millimeters of propagation, exceeding the time window supported by the buncher, further implying the importance of a highly integrated rebunching cavity. The electron bunch can be compressed to an even shorter bunch length, however limited by the mechanical constrains of the current setup, we cannot move the streaker to the designed position.

Ultrafast projection microscopy and diffraction

To demonstrate the performance of the setup, we performed the electron diffraction and microscopy experiment. Figure 6a-c show the high-quality diffraction signal from a crystallin silicon and the project microscopy imaging signal of a copper mesh, both collected with 0.5 s exposure time, implying the possibility of performing precision measurement with this all-optical THz-driven compact device. At the moment, the spatial resolution of the projection imaging is mainly limited by the sample position and the spatial resolution of the MCP detector (~100 μm), which can be further improved by reducing the gun-sample distance and increasing the sample-detector distance, hence the magnification factor. The strong field THz-driven photogun provides a new approach to generate higher energy, higher charge, highly controllable compact femtosecond point projection microscopy[5,47] and femtosecond energy electron diffraction[2].

In the meantime, benefiting from the high sensitivity of low energy electrons to field dynamics, we also demonstrated its capability of probing the ultrafast transient electric fields that build up at

the center of the copper mesh when irradiated by a laser pulse. We observe that at high pump fluence, the field from the plasma cloud is so strong that the electrons quickly smear out the shadow image of the copper mesh that shows a hole in the center [see supplementary material Fig. S4]. At relatively low fluence (20 mJ/cm^2), within the first few ps the inner part of electron beam moves to the center and outer part of the electron beam moves outwards indicating a donut shaped charged electron clouds formed after excitation (Fig. 6d). Afterwards, the diameter of the electron beam that passes through each clear hole on the copper mesh get increased. This implies the drainage of electrons after photoexcitation and a radial electric field developing from the positively charged ions on the mesh (Fig. 6e). The response of the electron beam to the transient plasma field implies the possibility of controlling the electron beam with well-designed laser-driven structures. This demonstrates the feasibility of a new microscope system in imaging of transient field dynamics near surfaces and paves the way for probing ultrafast charge carrier dynamics in nanostructures.

Conclusions and outlook

We have demonstrated a novel all-optical waveguide-based double THz-driven photogun with a movable tip-cathode and integrated multifunction segments enabling high precision control over the acceleration/manipulation phase and high beam quality. The tip provides a 10-fold enhancement of the field strength which reduces the THz-pulse energy required for acceleration. In addition, the tip's position adjustability allows tuning of the interaction length which reduces the demands on the fabrication precision which, for sub-millimeter scale of the components is currently at the edge of what is possible. The use of two counterpropagating THz pulses enables a clean electric field acceleration in the absence of magnetic deflection as well as a more homogeneous field distribution that helps to generate a high-quality electron beam. As the field-induced breakdown is expected to scale with the sixth root of the inverse THz pulse duration, with

the picosecond duration of the THz wave[24,25,48], using ~2×8 μJ of THz energy, the THz-driven photogun has demonstrated peak acceleration fields of ~3 GV/m, which is the highest ever reached in a photogun, leading to acceleration of electrons up to 14 keV. The generated electron beam can be focused down to <90 μm beam diameter with a transverse emittance of <0.015 mm mrad. With an integrated rebunching cavity, the electron bunch is further compressed down to 167 fs. The system also showed high stability and the ability to run for several weeks without any degradation at the levels of THz energy and UV laser power used. The high-quality electron beam enables us to perform first application in projection microscopy and diffraction. Such keV level low energy electron beam is also advantageous in gaining the field sensitivity. We were able to observe the transient plasma dynamics (positively and negatively charged ions) developed on the copper mesh after photoexcitation with high spatiotemporal resolution.

There remains, however, a lot of space for optimization of the gun design. For instance, the THz generation did not use cryogenic cooling of the Lithium Niobate crystal to increase conversion efficiency[49]. The first segment for electron emission is already close to the field emission threshold, integration of more segments to distribute the THz energy into successive layers can extend the acceleration distance, allowing for more efficient energy transfer from THz pulse to electrons. With sharper tips and larger emitter–detector distance, a resolution of a few nm is expected. Follow-up experiments may also include improved laser coupling, multilayer structure for both spatial and temporal manipulation[12], or new acceleration schemes such as acceleration with multicycle THz fields inside the cavity[50] or waveguide[13]. It is also expected that with millijoule-scale THz, which are feasible today, MeV electron pulses can be achieved with current solution [see supplementary material Fig. S2d].

The exceptional performance and compactness of such THz-based photoguns make them very attractive for pursuing ultrafast electron microscopy and diffraction at the few- to sub- fs range necessary for probing the fastest material dynamics. The high acceleration field gradient driven by short THz pulses makes it possible to minimize the initial blow-up of the emittance by space-charge forces, generate higher charge and support higher energy which can be beneficial for modern compact tip-based point projection electron guns[2,5], as well as improving brightness and bunch length for compact UED system[3]. Demonstration of a high-quality, all-optical THz-driven gun paves the way for future applications of THz-driven accelerator technology in radiation sources and ultrafast electron microscopy and diffraction.

Acknowledgements

The authors would like to thank Prof. Liejia Qian for support of the laser system and helpful discussions in this work. This work has been supported by the National Natural Science Foundation of China (Grant No.12174255), the Science and Technology Commission of Shanghai Municipality (Grant No. 22JC1401900), the Fundamental Research Funds for the Central Universities, European Research Council under the European Union's Seventh Framework Programme (FP7/2007-2013) through the Synergy Grant AXSIS (609920), the Cluster of Excellence 'Advanced Imaging of Matter' of the Deutsche Forschungsgemeinschaft (DFG) - EXC 2056 - project ID 390715994 and Project 655350 of the Deutsche Forschungsgemeinschaft (DFG) and the accelerator on a chip program (ACHIP) funded by the Gordon and Betty Moore foundation (GBMF4744). D.Z. would also like to thank the sponsorship from Yangyang Development Fund.

Author contribution

F.X.K., D.Z., and N.H.M. conceived and coordinated the project. J.Y., X.H., D.S., L.Z., and D.Z. designed the experimental setup and carried out the experiments with the help of J.M., and P.Y. on the laser systems. T.K., T.R., M.F., and G.K. contributed with helpful discussion on the THz photogun design and experiments. All authors contributed to writing the article, reading and approving the final manuscript.

Competing interests

The authors declare no competing interests**.**

Data availability

Data underlying the results presented in this paper may be obtained from the authors upon reasonable request.

Code availability

The code used in this paper is available from the corresponding author upon reasonable request.

Supplementary Information

Supplementary Fig. S1-S4.

References

1 Ischenko, A. A., Weber, P. M. & Miller, R. J. D. Capturing chemistry in action with electrons: realization of atomically resolved reaction dynamics. *Chemical Reviews* **117**, 11066-11124 (2017).

2 Gulde, M. *et al.* Ultrafast low-energy electron diffraction in transmission resolves polymer/graphene superstructure dynamics. *Science* **345**, 200-204 (2014).

3 Filippetto, D. *et al.* Ultrafast electron diffraction: Visualizing dynamic states of matter. *Reviews of Modern Physics* **94** (2022).

4 Zewail, A. H. 4D ultrafast electron diffraction, crystallography, and microscopy. *Annual Review of Physical Chemistry* **57**, 65-103 (2006).

5 Vogelsang, J., Hergert, G., Wang, D., Gross, P. & Lienau, C. Observing charge separation in nanoantennas via ultrafast point-projection electron microscopy. *Light Sci Appl* **7**, 55 (2018).

6 Bressler, C. & Chergui, M. Ultrafast X-ray absorption spectroscopy. *Chemical Reviews* **104**, 1781-1812 (2004).

7 Esarey, E., Schroeder, C. B. & Leemans, W. P. Physics of laser-driven plasma-based electron accelerators. *Reviews of Modern Physics* **81**, 1229-1285 (2009).

8 Malka, V. *et al.* Principles and applications of compact laser-plasma accelerators. *Nature Physics* **4**, 447-453 (2008).

9 Wang, W. *et al.* Free-electron lasing at 27 nanometres based on a laser wakefield accelerator. *Nature* **595**, 516-520 (2021).

10 Shiloh, R. *et al.* Electron phase-space control in photonic chip-based particle acceleration. *Nature* **597**, 498-502 (2021).

11 Sapra, N. V. *et al.* On-chip integrated laser-driven particle accelerator. *Science* **367**, 79-83 (2020).

12 Zhang, D. *et al.* Segmented terahertz electron accelerator and manipulator (STEAM). *Nature Photonics* **12**, 336-342 (2018).

13 Zhang, D. *et al.* Cascaded multicycle terahertz-driven ultrafast electron acceleration and manipulation. *Physical Review X* **10**, 011067 (2020).

14 Zhang, D. *et al.* Femtosecond phase control in high-field terahertz-driven ultrafast electron sources. *Optica* **6**, 872 (2019).

15 Tang, H. *et al.* Stable and scalable multistage terahertz-driven particle accelerator. *Physical Review Letters* **127**, 074801 (2021).

16 Hibberd, M. T. *et al.* Acceleration of relativistic beams using laser-generated terahertz pulses. *Nature Photonics* **14**, 755-759 (2020).

17 Curry, E., Fabbri, S., Maxson, J., Musumeci, P. & Gover, A. Meter-scale terahertz-driven acceleration of a relativistic beam. *Physical Review Letters* **120**, 094801 (2018).

18 Kroh, T. *et al.* Compact terahertz-powered electron photo-gun. *IPAC21* (2021).

19 Zhang, D. *et al.* Long range terahertz driven electron acceleration using phase shifters. *Applied Physics Reviews* **9**, 031407 (2022).

20 Hebling, J., Almasi, G., Kozma, I. & Kuhl, J. Velocity matching by pulse front tilting for large area THz-pulse generation. *Optics Express* **10**, 1161 (2002).

21 Fülöp, J. A. *et al.* Efficient generation of THz pulses with 0.4 mJ energy. *Optics Express* **22**, 20155 (2014).

22 Vicario, C., Monoszlai, B. & Hauri, C. P. GV/m single-cycle terahertz fields from a laser-driven large-size partitioned organic crystal. *Physical Review Letters* **112**, 213901 (2014).

23 Zhang, B. *et al.* 1.4 - mJ high energy terahertz radiation from lithium niobates. *Laser & Photonics Reviews* **15**, 2000295 (2021).

24 Dal Forno, M. *et al.* Experimental measurements of rf breakdowns and deflecting gradients in mm-wave metallic accelerating structures. *Physical Review Accelerators and Beams* **19**, 051302 (2016).

25 Wu, X. *et al.* High-gradient breakdown studies of an X -band compact linear collider prototype structure. *Physical Review Accelerators and Beams* **20**, 052001 (2017).

26 Jolly, S. W. *et al.* Spectral phase control of interfering chirped pulses for high-energy narrowband terahertz generation. *Nature Communications* **10**, 2591 (2019).

27 Zhang, D. *et al.* THz-Enhanced DC ultrafast electron diffractometer. *Ultrafast Science* **2021**, 1-7 (2021).

28 Snively, E. C. *et al.* Femtosecond compression dynamics and timing jitter suppression in a THz-driven electron bunch compressor. *Physical Review Letters* **124**, 054801 (2020).

29 Zhao, L. *et al.* Femtosecond relativistic electron beam with reduced timing jitter from THz driven beam compression. *Physical Review Letters* **124**, 054802 (2020).

30 Wimmer, L. *et al.* Terahertz control of nanotip photoemission. *Nature Physics* **10**, 432-436 (2014).

31 Matte, D. *et al.* Extreme lightwave electron field emission from a nanotip. *Physical Review Research* **3** (2021).

32 Li, S. & Jones, R. R. High-energy electron emission from metallic nano-tips driven by intense single-cycle terahertz pulses. *Nature Communications* **7**, 13405 (2016).

33 Fallahi, A., Fakhari, M., Yahaghi, A., Arrieta, M. & Kärtner, F. X. Short electron bunch generation using single-cycle ultrafast electron guns. *Physical Review Accelerators and Beams* **19**, 081302 (2016).

34 Ronny Huang, W. *et al.* Terahertz-driven, all-optical electron gun. *Optica* **3**, 1209 (2016).

35 Manz, S. *et al.* Mapping atomic motions with ultrabright electrons: towards fundamental limits in space-time resolution. *Faraday Discussions* **177**, 467-491 (2015).

36 Yang, J. *et al.* Imaging CF_3I conical intersection and photodissociation dynamics with ultrafast electron diffraction. *Science* **361**, 64-67 (2018).
37 Theuer, M., Shutler, A. J., Harsha, S. S., Beigang, R. & Grischkowsky, D. Terahertz two-cylinder waveguide coupler for transverse-magnetic and transverse-electric mode operation. *Applied Physics Letters* **98**, 071108 (2011).
38 Zou, Y., Cui, Y., Reiser, M. & O'Shea, P. G. Observation of the anomalous increase of the longitudinal energy spread in a space-charge-dominated electron beam. *Physical Review Letters* **94**, 134801 (2005).
39 Lange, S. L., Noori, N. K., Kristensen, T. M. B., Steenberg, K. & Jepsen, P. U. Ultrafast THz-driven electron emission from metal metasurfaces. *Journal of Applied Physics* **128**, 070901 (2020).
40 Hachmann, M. & Flöttmann, K. Measurement of ultra low transverse emittance at REGAE. *Nuclear Instruments and Methods in Physics Research, Section A: Accelerators, Spectrometers, Detectors and Associated Equipment* **829**, 318-320 (2016).
41 Qi, F. *et al.* Breaking 50 Femtosecond Resolution Barrier in MeV Ultrafast Electron Diffraction with a Double Bend Achromat Compressor. *Physical Review Letters* **124**, 134803 (2020).
42 Maxson, J. *et al.* Direct Measurement of Sub-10 fs Relativistic Electron Beams with Ultralow Emittance. *Physical Review Letters* **118**, 154802 (2017).
43 de Loos, M. J. *et al.* Compression of Subrelativistic Space-Charge-Dominated Electron Bunches for Single-Shot Femtosecond Electron Diffraction. *Physical Review Letters* **105**, 264801 (2010).
44 Kim, H. W. *et al.* Towards jitter-free ultrafast electron diffraction technology. *Nature Photonics* **14**, 245-249 (2020).
45 Zhao, L. *et al.* Terahertz Streaking of Few-Femtosecond Relativistic Electron Beams. *Physical Review X* **8**, 021061 (2018).
46 Li, R. K. *et al.* Terahertz-based subfemtosecond metrology of relativistic electron beams. *Physical Review Accelerators and Beams* **22**, 012803 (2019).
47 Müller, M., Paarmann, A. & Ernstorfer, R. Femtosecond electrons probing currents and atomic structure in nanomaterials. *Nature Communications* (2014).
48 Kilpatrick, W. D. Criterion for Vacuum Sparking Designed to Include Both rf and dc. *Review of Scientific Instruments* **28**, 824-826 (1957).
49 Huang, S.-W. *et al.* High conversion efficiency, high energy terahertz pulses by optical rectification in cryogenically cooled lithium niobate. *Optics Letters* **38**, 796 (2013).
50 Fakhari, M., Fallahi, A. & Kärtner, F. X. THz cavities and injectors for compact electron acceleration using laser-driven THz sources. *Physical Review Accelerators and Beams* **20**, 041302 (2017).
51 CST–Computer Simulation Technology, https://www.cst.com.

FIGURES

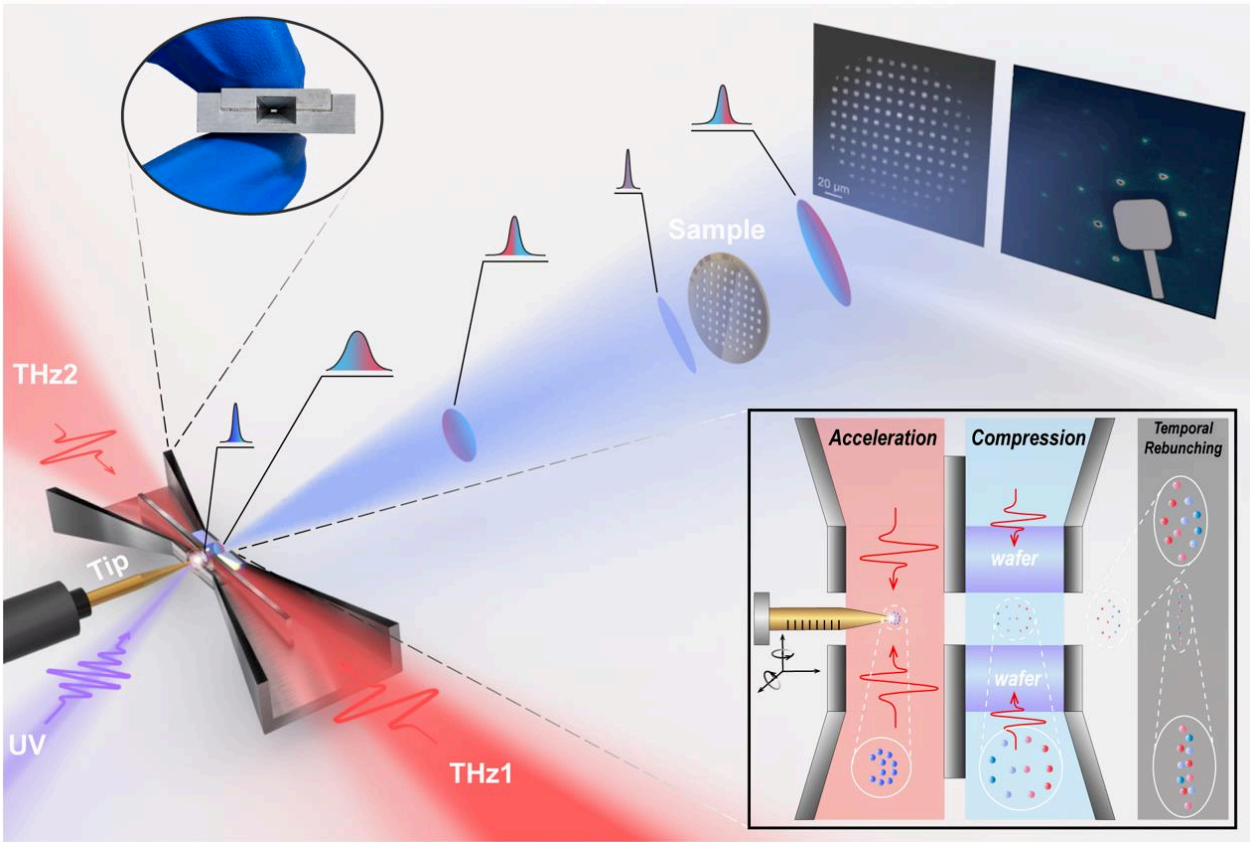

Fig. 1 Experimental setup. Two successive second harmonic generation stages in BBO crystals are used for the generation of 256 nm ultraviolet (UV) pulses from a Yb-Thin disc laser operating at 1030 nm. Two THz pulses generated by optical rectification in lithium niobate crystals are coupled into the THz gun by two PTFE convex lenses (CL). A solenoid is used to focus the electron bunch. The photoexcited electrons from the tip-cathode are accelerated by the THz field and then pass through the top anode aperture of the gun. Inset: enlarged view of the cross section of the THz gun.

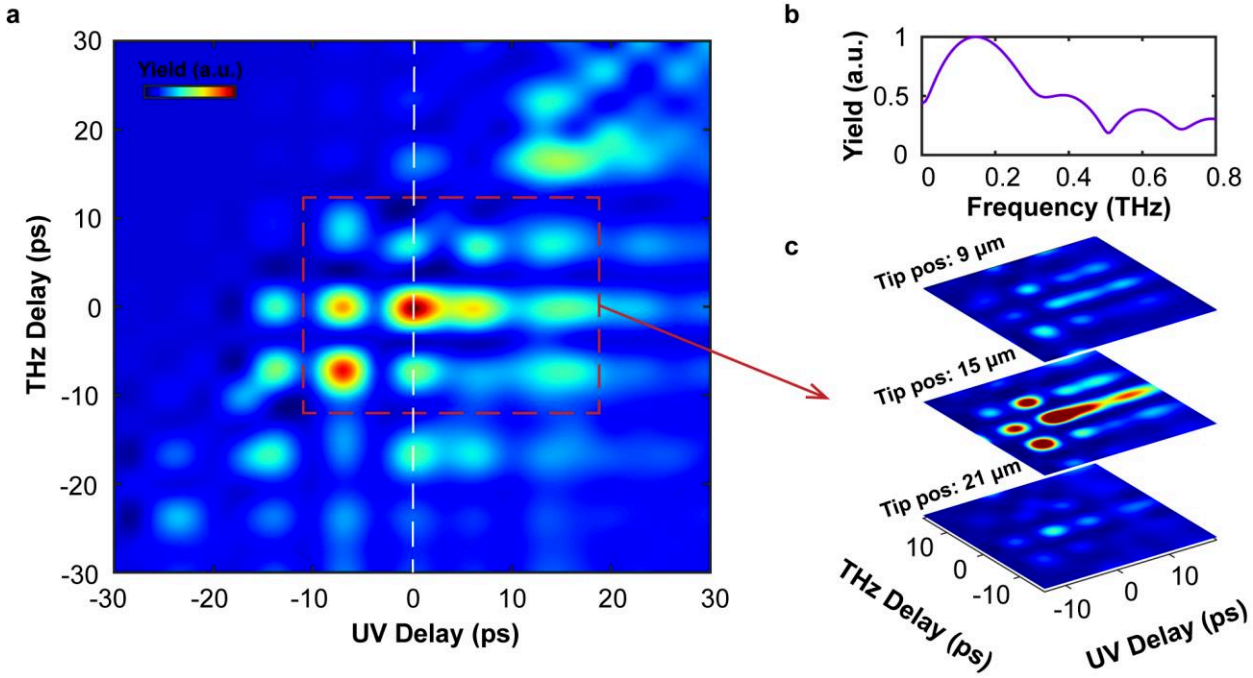

Fig. 2 Electron emission map measurement. a Emitted electron yield as a function of the relative delay between the UV and two THz pulses. **b** Fourier-transformed interference signal of the two THz pulses (white line in (a)). The center frequency of the THz pulses coupled into the gun is ~150 GHz. **c** Electron emission map measurement for different tip-cathode positions. The tip-cathode position represents the distance from the bottom layer of the gun to the front surface of the tip (Fig. 1).

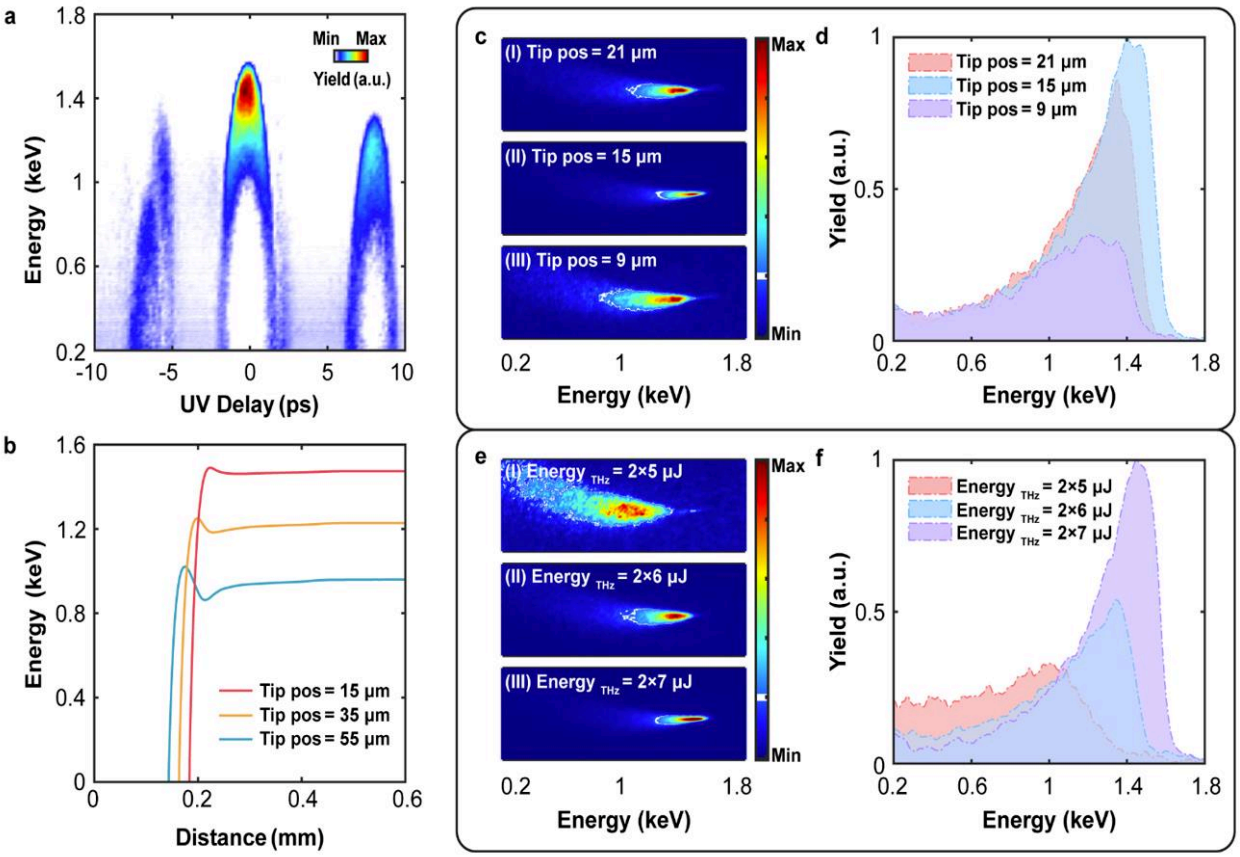

Fig. 3 Measured electron energy spectra. a Electron energy spectra as a function of UV delay with the two THz pulses fixed at zero-time delay with the magnetic field canceled according to Fig. 2. The color scale for each time delay has been adjusted to more clearly guide the eye over the center of mass changes in energy. Raw data of the spectra can be found in Fig. 3c and Fig.3e. **b** Evolution of maximum electron energy with acceleration distance at different tip-cathode position. **c,d,** Maximum energy gain measured with dipole magnet for different tip-cathode positions. The THz energy for these measurement was 2×6.5 μJ. **e,f,** Maximum electron energy with different driving THz energy.

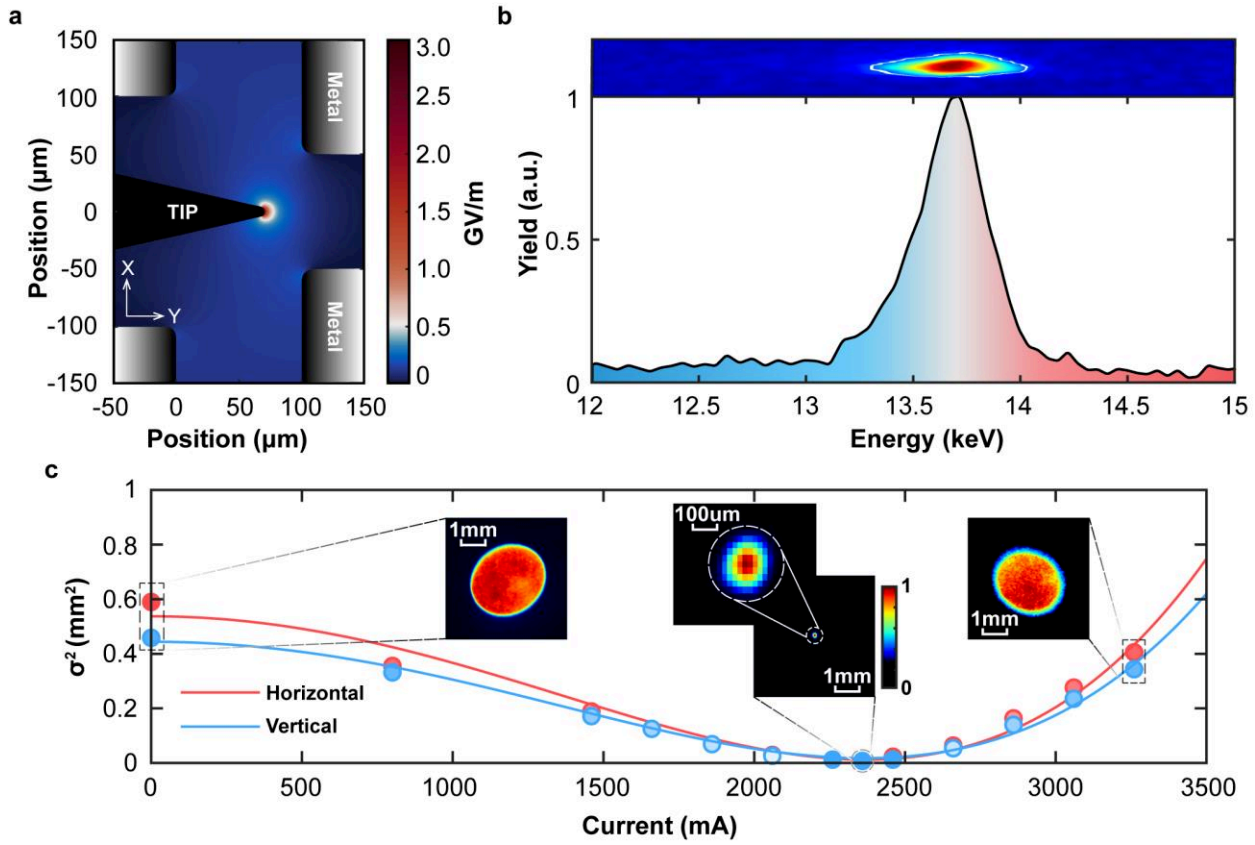

Fig. 4 Multifunction THz-driven device. a Cross section of the field distribution of a gun with a tip-cathode simulated with CST Microwave Studio[51]. **b** Maximum energy gain measured with dipole magnet. The THz energy for this measurement is 2×8 μJ with a 100 μm waveguide. **c** Measured root-mean-square beam size (σ) as a function of the magnetic field strength in the horizonal (x) direction and vertical (y) direction. For the x direction, $\varepsilon_{x,n} = 0.014\ mm\ mrad$ and for y direction, $\varepsilon_{y,n} = 0.015\ mm\ mrad$ (normalized emittance) are derived. Inset: spatial profile of the electron beam at the MCP detector.

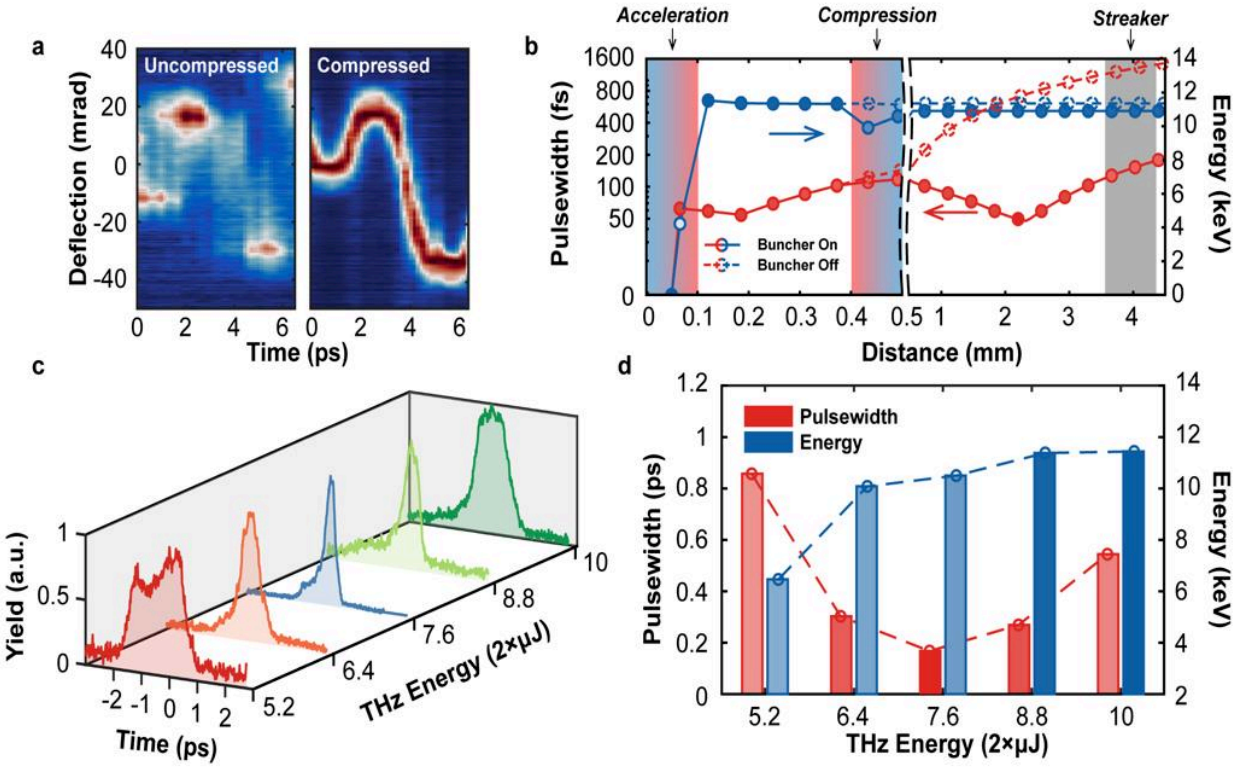

Fig. 5 Compression of electron bunch. a Time-dependent deflection diagrams measured by varying the delay between the arrival time of the electron bunch and the deflecting terahertz pulse for compressed and uncompressed electron bunches at different THz energy. **b** Simulated bunch length (red) in logarithmic scale and electron energy (blue) along the propagation direction with (solid circle) and without (dashed circle) the integrated rebunching layer. Measured electron temporal distribution (**c**), electron bunch length and energy (**d**) as a function of different THz energy.

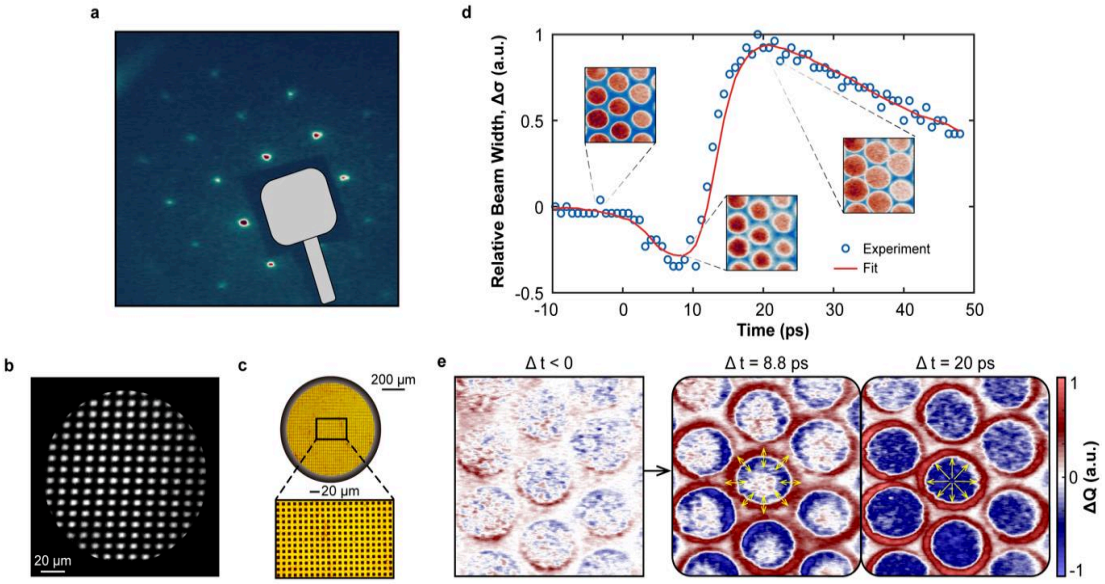

Fig. 6 Microscopy and diffraction. a Electron diffraction images of a 35 nm thick single-crystalline silicon film with a face-centered cubic structure. The data is collected by an MCP detector with 0.5 s exposure time**. b,c** Microscope images of the 2000 mesh grid measured with the THz gun (b) and optical microscope (c) for comparison. **d** Measured relative beam diameter change as a function of laser-electron delay time indicating the transient formation of the negatively charged electrons and positively charged ions. **e** Differential transmission images before (left) and after laser excitation. The yellow arrows indicate the plasmonic field direction built up by the charged particles after photoexcitation.